DESIGN AND PERFORMANCE OF THE NEW WIND TUNNEL IN THE FLUID MECHANICS LABORATORY AT THE UNIBW MÜNCHEN

O. Meyer*, C. Püchler*
* Universität der Bundeswehr München, 85577 Neubiberg, Germany

Abstract

A new 0.5 m x 0.5 m and 60 m/s subsonic wind tunnel of Göttinger type with closed test section is built in the Fluid Mechanics Laboratory of the Faculty of Mechanical Engineering at the Universität der Bundeswehr München. The preliminary power estimation of the planned tunnel is based on an existing NASA program, which accuracy is validated here against some existing large scale wind tunnels and their real working conditions. The space limitations in the laboratory lead to individual design solutions, for example a short and partially separating high speed diffuser where the suppression of separation is finally realised by a particular, intrusive flow element. The design of the sheet metal corner vanes is based on extensive CFD studies in addition to literature based experience. The entire wind tunnel is finally self built and about 90% of the material is based on hardware store equipment. The commissioning of the wind tunnel is accompanied by performance and flow quality measurements, the results of which will be presented.

Keywords

wind tunnel power estimation, wind tunnel design, diffuser optimisation, wind tunnel corner design, test section flow quality

NOMENCLATURE

Formula symbols

A_N	Cross Section Area of Nozzle Exit	m^2
AR	Aspect Ratio (exit to inlet area) of Diffuser	-
A_S	Cross Section Area of Settling Chamber	m^2
A_TS	Cross Section Area of Test Section	m^2
A_x/A_0	Aspect Ratio (exit to inlet area) of Diffuser	-
u	Wind Speed in x-Direction	m/s
c	Wind Speed	m/s
c_p	Pressure Coefficient	-
δ_1	Displacement Thickness of BL	m
Δp	Pressure Difference/Loss	Pa
η	Efficiency	-
A_FAN	Cross Section Area of Fan	m^2
κ	Contraction Ratio of Nozzle	-
λ	Wind Tunnel Factor	-
L_x/R_0	Ratio of Diffuser Length to Diffuser Inlet Width	-
N/W_i	Ratio of Diffuser Length to Diffuser Inlet Width	-
P_H	Hydraulic Power	W
Re	Reynolds Number	-
ρ	Air Density	kg/m^3
Tu	Turbulence Level	%
$\dot{V}$	Volume Flow	m^3/s
ζ	Pressure Loss Coefficient	-

Indexes

∞	Parameter in Test Section
tot	total
x,y,z	wind tunnel coordinate directions

Abbreviations

AVZ	BMW Aerodynamisches Versuchszentrum
BL	Boundary Layer
CFD	Computational Fluid Dynamics
EVZ	BMW Energietechnisches Versuchszentrum
EWK	BMW Energietechnischer Windkanal in EVZ
HSD	High Speed Diffuser
TE	Trailing Edge
UniBw M	Universität der Bundeswehr München

1. INTRODUCTION

A new wind tunnel for the education of students and for smaller research projects is being built in the Fluid Mechanics Laboratory of the Faculty of Mechanical Engineering at the UniBw M. The boundary conditions are given by the available space in the laboratory and the aerodynamic specification which can be summarised in table 1.
Other requirements include a minimum footprint in the laboratory and a certain simplicity of construction, as the wind tunnel has to be self-built as cheaply as possible. This leads

Parameter	Value	Unit
Max. Length	10.5	m
Max. Wind Speed	60	$\mathrm{m/s}$
Max. Height	4	m
Test Sect. Area	0.5 x 0.5	$\mathrm{m^2}$
Test Sect. Length	2	m
Max. Wind Speed Variation	± 0.5	$\%$
Turbulence Level	≤ 0.3	$\%$
Pressure Deviation in Cross Section	≤ 1	$\%$

TAB 1. Specification of new wind tunnel with closed test section

Parameter	Value	Unit
Diameter	0.9	m
Hub Diameter	0.5	m
Fan Power	21.94	kW
Motor Power	30	kW
Speed	1500	$1/\mathrm{min}$
Sound Pressure	106	dB
No. of Blades	12	-
Pressure Increase	1200	Pa
Fan Efficiency η	0.76	-
Volume Flow	50.000	$\mathrm{m^3/h}$
	14	$\mathrm{m^3/s}$

TAB 2. Technical data of TROX AXN 12/56/900 M-DFan

to a vertical design of the wind tunnel with the test section and fan on the ground and a mainly wooden construction with an aluminium supporting structure. This layout, with the settling chamber, test section and fan in a row on the floor, results in a short high speed diffuser behind the test section, which may separate. In addition, the corners will be designed based on a CFD study focusing on the pressure drop across the corners and the flow quality behind the corners as a function of several corner parameters (number, length and spacing of corner vanes). A further focus is on the design of the settling chamber (flow straightener, number and type of turbulence screens) and the nozzle shape (contraction ratio and contour) to achieve the specified flow quality in the test section. The power requirement to specify the correct fan is estimated once the preliminary design has been established. A NASA wind tunnel calculation program [1] will be used, which will first be validated against the real power requirements of several existing large wind tunnels. The NASA programme essentially calculates the pressure loss of all wind tunnel components and adds these to the total pressure loss from which the power requirement is derived.

2. FIRST POWER ESTIMATION

Estimating the likely power requirements of the facility is one of the first questions to be answered when designing a wind tunnel. The power plant is an expensive long lead item in wind tunnel construction and the required electrical power will determine the running costs of the facility. A first estimate is usually easy to make as the airflow (or hydraulic) power is defined by

$$P_{\mathrm{H}} = \Delta p \cdot \dot{V} \tag{1}$$

where Δp is the pressure difference in a flow (loss or gain). $\dot{V}$ is the volume flow $c \cdot A$. The aerodynamic power of the flow in the test section is therefore defined by the specified flow velocity c and the cross-sectional area A in the test section. However, in an Eiffel type wind tunnel (open inlet and open outlet) the fan must provide the dynamic pressure of the flow plus any pressure drop along the duct. The pressure requirement in a Göttinger type wind tunnel (closed circuit) is only caused by the pressure losses in the circuit once the flow is accelerated and steady. The pressure requirement is usually expressed as a multiple of the dynamic pressure in the test section,

$$P_{\mathrm{H}} = \zeta \frac{\rho}{2} c_\infty^2 \cdot \dot{V} = \zeta \frac{\rho}{2} c_\infty^3 \cdot A_{\mathrm{TS}} \tag{2}$$

with the pressure loss coefficient ζ, which becomes an 'aerodynamic quality factor' in wind tunnel design. The wind speed c_∞ and the cross sectional area A_{TS} are now defined in the test section. This can also be thought of as the power to be put into the airflow, and the pressure loss coefficient can then be defined as the tunnel power factor, also called λ, see [2]. The fan shaft input power can be estimated by dividing equation 2 by the fan efficiency η_{Fan}.

$$P_{\mathrm{Fan}} = \frac{\zeta \cdot \rho \cdot c_\infty^3 \cdot A_{\mathrm{TS}}}{2 \cdot \eta_{\mathrm{Fan}}} \tag{3}$$

Typical values for ζ vary between $0.15 \leq \zeta \leq 0.4$ for closed loop wind tunnels with closed test sections and $0.45 \leq \zeta \leq 0.8$ for closed loop wind tunnels with open jet test sections. Eiffel type wind tunnels show a range of $1.2 \leq \zeta \leq 1.9$, [1], [3], [4]. Typical fan efficiencies can be found in the range of $\eta_{\mathrm{Fan}} = 55\%$ for simple industrial fans and up to about $\eta_{\mathrm{Fan}} = 90\%$ for optimised wind tunnel fans.
Given the specification, table 1, a $\zeta \approx 0.25$, an expected mean fan efficiency of $\eta_{\mathrm{Fan}} = 70\%$ and an air density of $\rho = 1.13\mathrm{kg/m^3}$, a first power estimate leads to a fan power of $P_{\mathrm{Fan}} \approx 11\mathrm{kW}$. If we add a safety margin to the tunnel factor ζ due to probable inaccuracies in construction quality (leaks, steps, roughness, design challenges), set it to $\zeta = 0.4$, and add a speed safety margin of $\Delta c_\infty = +5\mathrm{m/s}$, the required fan power may be estimated as $P_{\mathrm{Fan}} \approx 20.5\mathrm{kW}$.

3. COMPONENT DESIGN

3.1. Fan and Transition Elements

The fan selection is usually based on the required volume flow $\dot{V}$ and pressure rise Δp across the fan. With the above assumptions we can estimate a $\Delta p \approx 1000\mathrm{Pa}$ and a volume flow of $\dot{V} = 16\mathrm{m^3/s}$. For this project a TROX AXN 12/56/900 M-D fan with outlet guide vanes is selected which meets the above performance requirements, see table 2. However, the nominal air flow rate is lower, but the possible pressure rise is higher. It is assumed that the parameters can be adjusted, if necessary, during commissioning of the wind tunnel by adjusting the inclination of the fan blades.
According to [3], a fan to test section area ratio of 2 or 3 to 1 is recommended. The current selection gives a fan to test section area ratio of $\mathrm{A_{Fan}/A_{TS}} = 2.55$. The fan is mechanically decoupled from the ground by damping elements and from the airline by elastic fabric sleeves to minimise the in-

troduction of vibrations into the wind tunnel structure. The entire airline will have rectangular cross-sections, so there must be transition elements from rectangular to circular to the fan and vice versa from the fan. These transition elements are designed to keep the cross sectional area constant, i.e. from the fan diameter of $0.9\mathrm{m}$ the elements transition over a distance of $0.5\mathrm{m}$ to $0.8\mathrm{m} \times 0.8\mathrm{m}$ rectangular.

3.2. Test Section

The cross-sectional area is defined as 0.5m x 0.5m to accommodate the planned tests. The length of the test section should be between 2.5 and 3.0 times the hydraulic diameter of the test section if wind tunnel wall corrections are to be made using a wall pressure signature method, [5]. Since this should be an option, and since the test section also needs to be of sufficient length for a likely application of adaptive walls, the relative length should be even greater: it is described in [6] for the application of single step wall correction methods with 2D adaptive walls that any model perturbations should be zero at the inlet and outlet of the test section. The fact that the model blockage can be larger in adaptive wall test sections than in solid wall test sections is taken into account by setting the length to 4.0 hydraulic diameters, i.e. 2m.
In addition, the straight walls should be inclined in flow direction to compensate for boundary layer growth and thus maintain a constant axial pressure in the empty test section. Therefore, the required displacement at the end of the test section is calculated using the displacement thickness for turbulent boundary layers on a flat plate according to [7]:

$$\delta_1 = 0.048 \frac{x}{\sqrt[5]{Re_x}}. \tag{4}$$

For the given test section length and a wind speed of $50\mathrm{m/s}$, $\delta_1 = 4\mathrm{mm}$ is calculated at the end of each wall. It is explained in [8] that it is sufficient to displace two walls to achieve a 3D flow correction, i.e. the wall end displacements for the top and bottom walls are set to 8mm each to compensate for the total boundary layer growth and thus ensure a constant velocity in the test section. The side walls are kept parallel.
Air vents are located at the end of the test section to allow tests to be carried out at ambient pressure. This means that the rest of the wind tunnel is pressurised during testing.

3.3. Settling Chamber (Flow Straightener and Screens)

The settling chamber with flow straightener and turbulence screens as well as the nozzle are main contributors to the flow quality in the test section. There is a trade-off between the contraction ratio of the nozzle, which determines the size of the total airline, the pressure losses in the airline and the specified flow quality. The higher the contraction ratio, the larger the wind tunnel, the lower the pressure losses and the better some of the flow parameters in the test section. Initial sketches of the airline show that a nozzle contraction ratio of $\kappa = A_S/A_N = 6$ is the maximum possible to stay within the space constraints in the laboratory and still accommodate reasonable diffusers.
The settling chamber has a cross section of 1.225m x 1.225m with the nozzle contraction ratio set to $\kappa = 6$. The length of the settling chamber is determined by the number of turbulence screens and the required spacing between the settling chamber components. Firstly, a certain distance from the flow straightener (honeycomb) to the exit of corner 4 should be maintained to allow the corner vane wake to dissipate before the flow enters the honeycomb. The honeycomb should have approximately 25,000 cells according to [2] and [3] with a cell length to diameter ratio of 6 to 8. A sheet steel honeycomb with a cell diameter of $6.4\mathrm{mm}$ and a length of $51.2\mathrm{mm}$ is selected, resulting in approximately 35,000 cells in the cross section and a cell length to diameter ratio of 8. Three screens are placed behind the honeycomb in the settling chamber to reduce turbulence. The screens have a wire diameter of $0.4\mathrm{mm}$ and a wire spacing of $1.3\mathrm{mm}$, giving a pressure loss coefficient of $\zeta = 1.96$ for each screen according to [9]. The screen spacing should be 500 times the wire diameter, [3], giving a spacing of $200\mathrm{mm}$.
The expected turbulence reduction from the three screens and the contraction can be estimated from [3]. The turbulence level in the test section also depends on the assumed turbulence level in front of the screens. A turbulence level of $Tu_{x,y,z} \leq 0.1\%$ in the test section can be estimated with an assumed turbulence level of $Tu = 5\%$ before the screens.

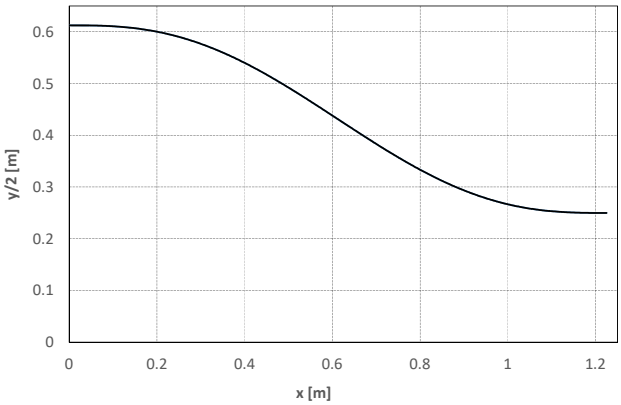

FIG 1. Contour of nozzle

3.4. Nozzle

Nozzle design is usually one of the most important parts of the wind tunnel design as it is the last component before the flow enters the test section. Therefore, the flow quality in the test section is directly influenced by the nozzle flow. The possible contraction is already defined to be $\kappa = 6$ and the length should be small due to space constraints in the laboratory. The work in [10] focuses on the design of nozzles for small low speed wind tunnels and recommends a 5^{th} order polynomial function, see equation 5. The application of this function results in a nozzle with a length to height ratio of 1, an inflection point at $x/l = 0.5$ and a contour as shown in the figure 1.

$$y(x) = h_i + (h_i - h_e) \cdot \left(-10x^3 + 15x^4 - 6x^5\right) \tag{5}$$

The nozzle is finally build from wooden panels by an external carpenter.

3.5. High Speed Diffuser, HSD

The position of the fan should be on the floor for ease of construction and the airline should be vertical for a minimum footprint in the laboratory, see chapter 1. However, these constraints, together with the now designed settling chamber, nozzle, test section and fan transition parts, result in a relatively short transition from the test section to the fan. And therefore a relatively steep diffuser, which may sepa-

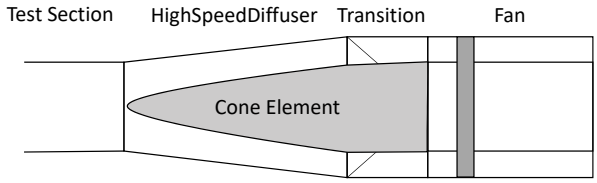

FIG 2. Cone element in high speed diffuser

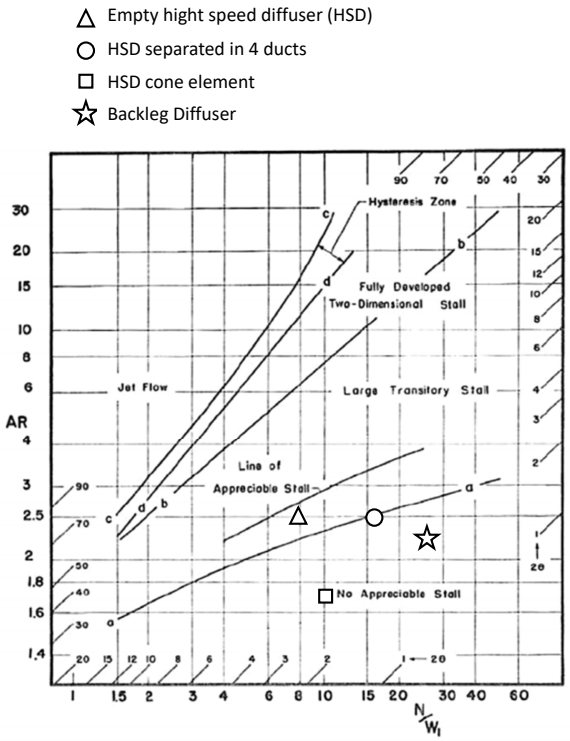

FIG 3. Flow regimes in straight-wall, two-dimensional diffusers, based on [11]

rate, see also the sketch in fig. 5. A wide angle diffuser may solve the space problem, but the additional pressure losses due to additional screens should be avoided. Several measures are considered to avoid flow separation, such as turbulator strips, division of the diffuser duct into four ducts, and an intrusive flow element (cone) to direct the flow to the fan with uniform and minimum opening ration, fig.2.

Figure 3 shows the flow regimes in 2D straight wall diffusers characterised by the geometry, [11]. The 2D diffuser is characterised by the aspect ratio $AR = \frac{A_x}{A_0}$, i.e. the ratio of the outlet area to the inlet area of the diffuser and the ratio of the diffuser length N to the inlet width W_i. The triangle in the diagram shows the expected flow regime for the empty diffuser, i.e. this will be close to "appreciable stall" and well above the line a–a which marks the start of stall. With a vertical and horizontal splitter plate, the diffuser is divided into four less critical ducts. The aspect ratio remains constant, but the relative length increases. The dot marks this less critical configuration, but still on the stall line a–a. Adding a body of revolution (cone) inside the diffuser directs the flow to the fan blade ring area, square in diagram, which is well below the critical line a–a.

A comprehensive CFD study was carried out in [12] to investigate the flow behaviour in a 3D square diffuser as used here. The results are shown in fig. 4 and confirm the results shown in fig.3.

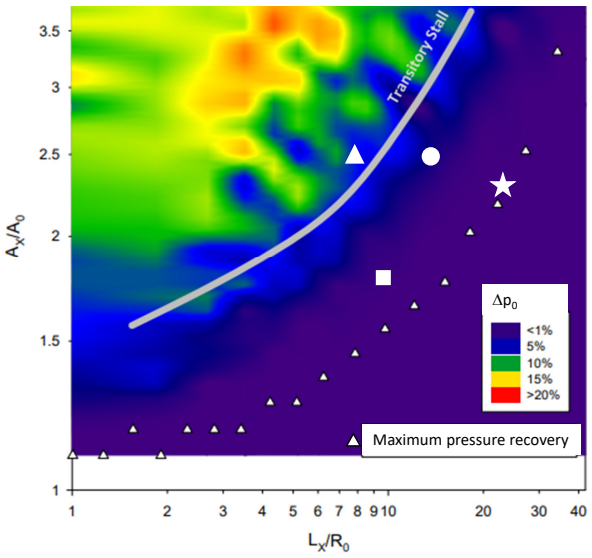

FIG 4. Flow regimes in straight-wall, three-dimensional quadratic diffusers, based on [12]

A detailed discussion of the high-speed diffuser design will be part of a future publication including the analysis of separation areas and pressure loss of the different designs. However, flow investigations by wool tuft visualisation have shown that flow separation occurs without any precaution and can be successfully avoided by the conical element that will be added to the high speed diffuser.

3.6. Backleg Diffuser

The backleg diffuser is much less critical than the high-speed diffuser because the available length is sufficient to open the area from corner two to the final area of the settling chamber without separation. This means that the maximum cross section area in the wind tunnel is achieved at the end of the diffuser and the start of corner three. The expected flow regimes are also marked with a star in figures 3 and 4, which show a certain distance to the onset of flow separation. Fig. 4 also shows that this diffuser design can probably provide the maximum possible pressure recovery in this section.

3.7. Corners

The design of the corners is based on both literature and an additional CFD study, the details of which will be part of another publication. In principle, bended sheet metal vanes should provide sufficient flow quality for this project. However, a CFD study showed that the geometric parameters of the turning vanes influence the flow quality behind the corner and the pressure drop across the corner in such a way that a careful decision about the corner vane parameters should be made based on the flow requirements behind a corner. For example, a higher number of vanes may improve the flow quality behind the corner, but may cause a higher total pressure loss due to increased friction. Therefore, a trade-off between these two requirements must be found. The CFD-study also showed that it is very important to use vane extensions, i.e. a straight extension of the trailing edge with a length of appr. 25% of the vane radius. This increases the circulation and the effectiveness of the flow re-direction. The corners have the same inlet and outlet area each, i.e. they are not diffusing. The realised corner parameters are listed in table 3.

Corner	1	2	3	4
Number of Vanes	12	14	10	13
Radius	10cm	10cm	25cm	25cm
Vane Spacing	8.7cm	7.5cm	15.7cm	12.4cm
Vane Cord	14.1cm	14.1cm	35.4cm	35.4cm
Vane TE Extension	2.5cm	2.5cm	6.3cm	6.3cm

TAB 3. Corner parameters

4. DETAILED PERFORMANCE ESTIMATION

The expected power requirement of the wind tunnel under the specified conditions can be estimated more accurately once the basic design of the tunnel is known. Each part of the wind tunnel is pre-designed either according to known standards or by individual detailed pre-design (high speed diffuser and corners). The pressure loss factor ζ can be calculated for each component and summed over all parts of the wind tunnel to give the complete airline. This procedure is generally summarised in a program presented in [1], which is used here.

The program uses well-known standard ζ calculation procedures, which can be found, for example, in [9]. The program uses the wind tunnels individual dimensions of each wind tunnel element, the atmospheric boundary conditions under test and the specified wind tunnel performance (planned wind speed or available power).

4.1. Validation of Performance Calculation Program

A study using data from several existing full-scale wind tunnels was carried out to validate the general suitability and accuracy of the program. Actual performance data during wind tunnel operation was recorded and compared with the calculation based on real wind tunnel dimensions, component details and environmental conditions. The wind tunnels studied were

a) BMW EVZ-EWK, an environmental simulation wind tunnel of the Energie- und umwelttechnisches Versuchszentrum (EVZ) of BMW in Munich with 3/4 open test section and an area of $8.4\mathrm{m}^2$. Several test conditions were investigated. The total pressure drop across the heat exchanger and the flow straightener in the program were taken from measurements. The $3/4$ open test section is accounted for in the calculation by $3/4$ shear layer loss and boundary layer development on the bottom wall. The temperature was set to $25^{\circ}\mathrm{C}$ and the test section was empty.
b) BMW AVZ-1:1 Windkanal, the large BMW aerodynamic wind tunnel of the Aerodynamisches Versuchszentrum (AVZ) with a 3/4 open test section with an area of $25\mathrm{m}^2$. The test section was empty. The total pressure drop across the heat exchanger and the flow straightener in the program were taken from measurements, the total pressure drop across the FOD screen was estimated.
c) The BMW AVZ-AeroLab, the smaller BMW wind tunnel of the Aerodynamic Test Centre with a 3/4 open test section and $14\mathrm{m}^2$ cross-section. The investigation was carried out with a full scale model in the test section. The total pressure drop across the heat exchanger and flow straightener in the programme was taken from measurements, the total pressure drop across the FOD screen was estimated.
d) RUAG LWTE, the large wind tunnel in Emmen with closed test section and $32.5\mathrm{m}^2$ cross section. The test was performed with an empty test section.

WT	Conditions	Power	Dev.	ζ
BMW	$250\mathrm{km/h}$			
EVZ	measurement	1250kW		
EWK	calculation	1212kW	-3%	0.66
BMW	$200\mathrm{km/h}$			
EVZ	measurement	676kW		
EWK	calculation	680kW	0.6%	0.73
BMW	$100\mathrm{km/h}$			
EVZ	measurement	95.2kW		
EWK	calculation	87.7kW	-8.6%	0.74
BMW	$60\mathrm{km/h}$			
EVZ	measurement	21.3kW		
EWK	calculation	19.3kW	-10.4%	0.75
BMW	$200\mathrm{km/h}$			
AVZ	measurement	1612kW		
1:1	calculation	1551kW	-4%	0.55
BMW	$140\mathrm{km/h}$			
AVZ	measurement	512kW		
1:1	calculation	545kW	6%	0.55
BMW	$280\mathrm{km/h}$			
AVZ	measurement	2250kW		
AeroL	calculation	2304kW	4.4%	0.54
BMW	$140\mathrm{km/h}$			
AVZ	measurement	269kW		
AeroL	calculation	299kW	10%	0.55
RUAG	$245\mathrm{km/h}$			
LWTE	measurement	2789kW		
	calculation	2968 kW	6%	0.38

TAB 4. Comparison of calculated and real WT power consumption

The results are listed in the table 4. The fan efficiency is an important parameter that directly affects the results. However, the fan map has not been taken into account and instead the fan efficiency has been set to a constant value of $\eta_{\mathrm{Fan}} = 0.89$. This may explain the variation in prediction accuracy with wind speed. But the deviation in the prediction is very small ($\leq 10\%$) if a reasonable operating point is chosen. Otherwise, the individual fan maps should be considered and the realistic fan efficiency should be used to further improve the prediction accuracy.

4.2. Power Estimation and Power Requirement of new Wind Tunnel

The design details of the wind tunnel can be added to the NASA programme for a detailed calculation of the wind tunnel performance once the design of the wind tunnel components and the airline is finalised. The design based on the initially described boundary conditions given by the laboratory dimensions and a low-cost self-build construction is shown in figure 5. The detailed input and output data are given in Appendix A and show very good agreement with the initial power estimation in chapter 2. The pressure loss

coefficient $\zeta = \frac{\mathrm{d}p}{q}$ is estimated to $\zeta = 0.38$ resulting in a required fan power of $P_{\mathsf{Fan}} = 18\mathrm{kW}$.
In the meantime the wind tunnel is commissioned and data are available. The maximum achievable wind speed is $c_\infty = 61.8\mathrm{m/s}$ at the maximum rotational speed of the fan $(1500\mathrm{RPM})$. The measured pressure increase over the fan is $\mathrm{d}p = 895\mathrm{Pa}$. With a corresponding dynamic pressure in the test section of $q_\infty = 2100\mathrm{Pa}$ the wind tunnels loss coefficient calculates to $\zeta = 0.426$.
The deviation from theory and wind tunnel measurement can be explained by leakages between the various wind tunnel elements. The sealing of the wind tunnel will be one of the major refinishing actions. The sealing problem is obvious when blowing smoke into the airline. However, the requirement of a wind speed of $c_\infty = 60.0\mathrm{m/s}$ is met and it showed, that the initial safety margins were properly chosen.

5. FLOW QUALITY

5.1. Axial Pressure Distribution

The axial static pressure distribution is measured by a pitot static probe through a longitudinal slot in the ceiling of the test section. The probe is connected to a Chell μDAQ-64DTC-Q pressure scanner. Positioning is provided by an ISEL 2-axis traverse mounted permanently at the top of the test section. The wind speed is set to $50\mathrm{m/s}$. The reference pressures p_∞ and q_∞ are taken from the wind speed control which is calibrated to the centre of the test section, see chapter 5.5. The axial static pressure distribution is shown in fig. 6 as $c_p[\%]$, see equation 6. The axial distribution of the pressure coefficient c_p shows a constant flow velocity in this area. The visible variation in c_p corresponds to a local static pressure deviation of appr. $\pm 1\mathrm{Pa}$. Other measurements showed static pressure deviations of up to $\pm 3\mathrm{Pa}$ at $50\mathrm{m/s}$, which can be attributed to uncertainties in pressure measurement.

$$c_{p,x} = \frac{p_x - p_\infty}{q_\infty} \cdot 100\% \tag{6}$$

Another parameter to evaluate the constancy of the axial wind speed is the axial pressure gradient dc_p/dx. This parameter is not applicable here as the wind speed appears to be virtually constant in the test section.
Important is the proof of the correct wall inclination angle which was set according to chapter 3.2 for a wind speed of $50\mathrm{m/s}$. The constant axial pressure shows that the wall angle is correct for this speed.

5.2. Flow Uniformity, Cross Sectional Pressure Distribution

Flow uniformity is analysed by measuring the pressure distribution in the cross-sectional area at the centre of the test section with a static pitot probe. Positioning is achieved using a traverse system in the vertical direction at different positions through the test section ceiling. The measurement grid extends from about $-200\mathrm{mm}$ to about $200\mathrm{mm}$ in both lateral and vertical directions, see fig. 7. The pressure variation is again expressed as the pressure coefficient $c_p[\%]$, i.e. the difference between the local static pressure and the static pressure at the centre of the test section (reference position) related to the dynamic pressure of the flow at the reference position, see equation 7.

$$c_{p,yz} = \frac{p_{yz} - p_\infty}{q_\infty} \cdot 100\% \tag{7}$$

Figure 7 shows the pressure variation in the reference area of the test section at $50\mathrm{m/s}$. The variation is approximately $c_p = \pm 0.2\%$ in the main centre area. The location of the maximum deviation of about $c_p = -0.8\%$ is in the lower right area of the test section floor. However, the remaining area of the test section shows only minor deviations. A very important result is that the wake of the fan hub is not present in the test section because the fan hub with a diameter of $0.5\mathrm{m}$ is operated without a rear cone due to the cooling requirements of the hub mounted motor.
The vertical centreline at $x, y = 0\mathrm{mm}$ is additionally investigated by a detailed pressure measurement with a pitot static probe positioned by the traverse at a wind speed of $40\mathrm{m/s}$. Fig. 8 shows the velocity profile $u(z)$. The wake of the fan hub is not visible, but there is a slight overspeed above the upper and lower boundary layers. This overspeed is caused by the wall interference as the probe approaches the wall. The relative velocity variation is $\Delta u_z/u_0 \pm 0.1\%$ in the main flow outside the boundary layers, see fig. 9.

5.3. Turbulence Level

The turbulence level, equation 8, is determined at the reference position using a 1D hot wire probe and a Dantec CTA system at wind speeds of $20, 30$ and $40, \mathrm{m/s}$. Preliminary results indicate a turbulence level of $Tu = 0.38\%$ with a low pass filter set at $10\mathrm{kHz}$. However, it has not yet been possible to repeat the measurements as the wooden tunnel still suffers from wood chips in the airline, which prevents the use of hot wires in the test section for an extended period of time.

$$Tu = \frac{\sqrt{\overline{u^2}}}{u_\infty} \tag{8}$$

5.4. Sound Pressure Level

The sound pressure level is measured to assess the working conditions in the laboratory. The measurement position is next to the test section at a distance of $1\mathrm{m}$ in the area of the test section reference point. The measurement is carried out with a Brüel& Kjaer free-field microphone and a mobile SQuadriga II DAQ system from HEAD acoustics. Initially, the noise from the electric converter of the WT motor dominates, until the wind tunnel becomes the dominant noise source above $10\mathrm{m/s}$, see fig. 10. The sound pressure level is averaged over time as the sum of all frequencies with an (A) weighting. Workplace regulations require hearing protection at sound pressure levels above $85\mathrm{dBA}$, which is given above a wind speed of $50\mathrm{m/s}$.

5.5. Flow Speed Measurement and Control Accuracy

The self-built wind tunnel incorporates a self-programmed wind tunnel control system which allows wind speed control and fan speed adjustment. Wind speed control is achieved using the nozzle method and calibration at the test section reference point (test section centre). The nozzle method consists of four circumferential static measurements in the settling chamber (p_{SC}) and four at the nozzle exit (p_{NE}), each connected by a ring pipe and pneumatically averaged. The calibration factor k is determined by a q_∞-measurement at

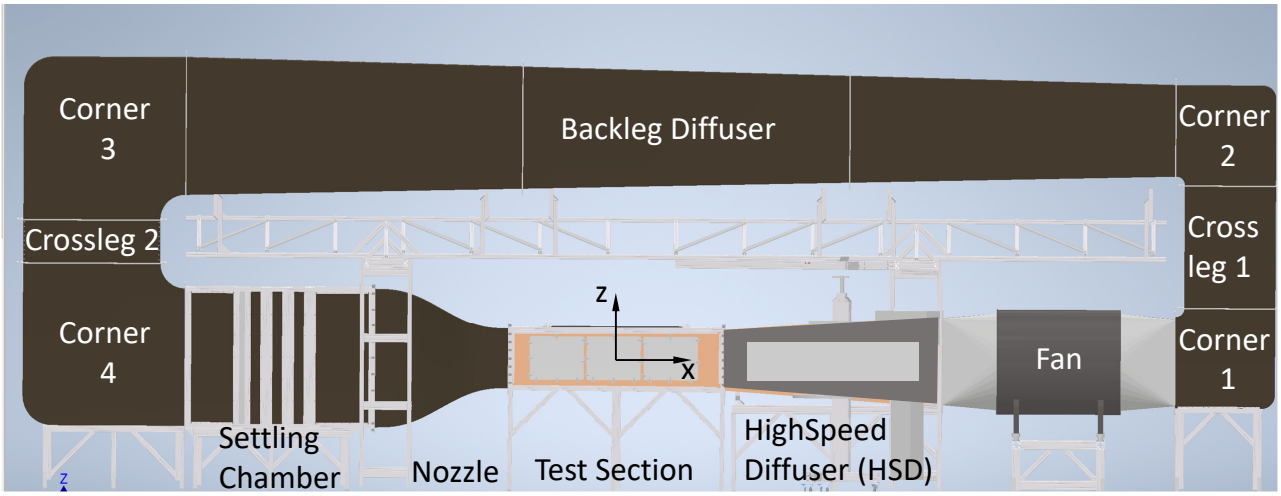

FIG 5. Sideview of wind tunnel

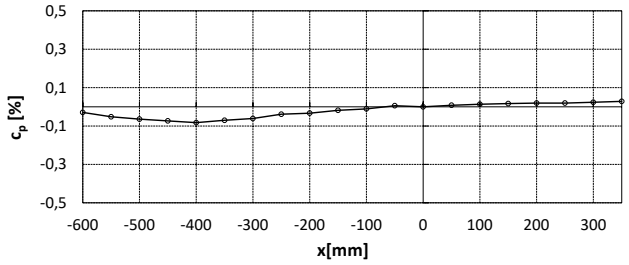

FIG 6. Axial distribution of static pressure coefficient c_p in the test section at $50\mathrm{m/s}$

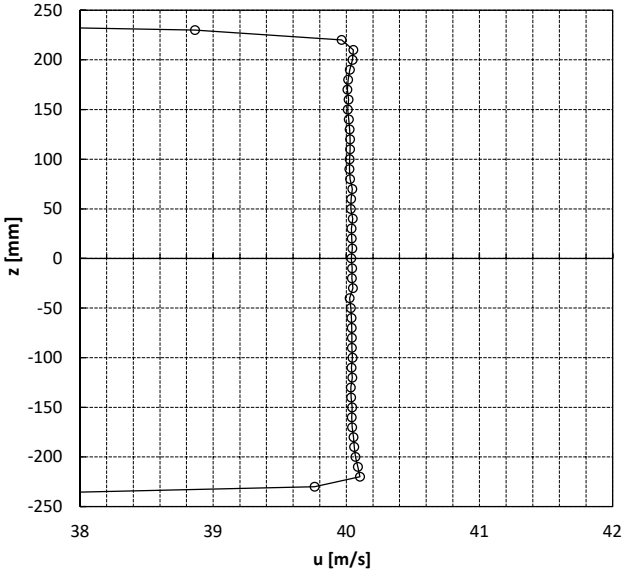

FIG 8. Vertical velocity distribution at $40\mathrm{m/s}$ at the test section centre

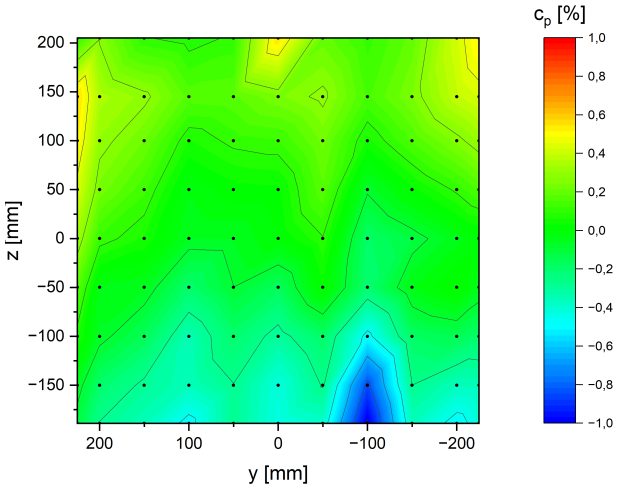

FIG 7. Flow uniformity, variation in static pressure coefficient c_p at $50\mathrm{m/s}$

the reference position with a pitot static probe. The calibration factor is determined by the equation 9 to $k = 1.024$.

$$k = \frac{q_\infty}{p_{\mathrm{SC}} - p_{\mathrm{NE}}} \tag{9}$$

The wind speed is calculated using the equation 10 with the measured flow temperature T_∞ and ambient pressure p_∞. The ambient pressure corresponds to the static pressure in the test section due to the test section ventilation.

$$c_\infty = \sqrt{\frac{2RT_\infty}{p_\infty} k \left(p_{\mathrm{SC}} - p_{\mathrm{NE}}\right)} \tag{10}$$

The speed control shows a very accurate and stable regulation of the wind speed, here recorded and displayed over $300\mathrm{s}$ at $20\mathrm{Hz}$, see figure 11. The upper figure shows the speed measurement using a pitot static probe at the reference point taken from the raw pressure signals recorded at $20\mathrm{Hz}$. The lower figure shows the same measurement, but the results are shown with a $1\mathrm{s}$ floating average applied to visualise the constancy of the speed control. The speed variation over time corresponds to $u_{\mathrm{RMS}} = 0.03\mathrm{m/s}$

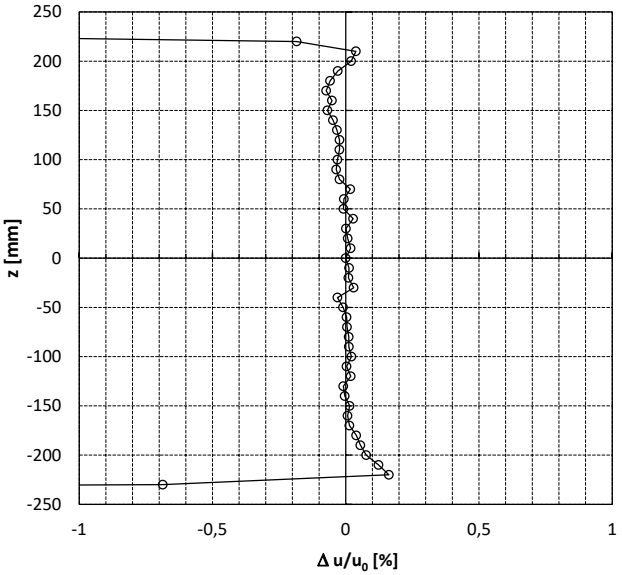

FIG 9. Relative vertical deviation of u_z from reference point at $40\mathrm{m/s}$ at the test section centre

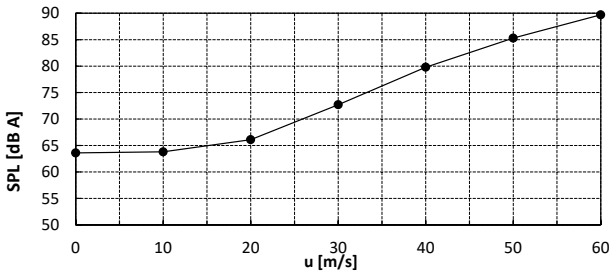

FIG 10. Sound Pressure Levels (sum, A-weighted) $1\mathrm{m}$ beside test section in laboratory

or 0.06%. The average wind speed deviation from the setpoint shows a negligible deviation in the reference position of less than $0.01\mathrm{m/s}$ at a setpoint of $50\mathrm{m/s}$ which is less than 0.02%.

6. CONCLUSION

The wind tunnel fits into the available space in the laboratory and is entirely self designed and self built. Only the nozzle was built by an external carpenter. The initial specification lead via a first power estimation to a fan, which finally met the initial wind speed requirement in the wind tunnel. The NASA wind tunnel power estimation tool was validated against several large scale wind tunnels and proved to work in within an accuracy of $\pm 10\%$ or better. The flow quality with respect to the axial and vertical distribution of pressure/speed is very good with a speed variation $u < \pm 0.1\%$ in the measured points. Any wake of the fan hub is not present in the test section, the flow is undisturbed and even. The wind speed control is very accurate and stable at the calibration speed of $50\mathrm{m/s}$ in the reference point and also with a very low variation. The turbulence level measurement must be confirmed once the debris in the wind tunnel has been reduced.

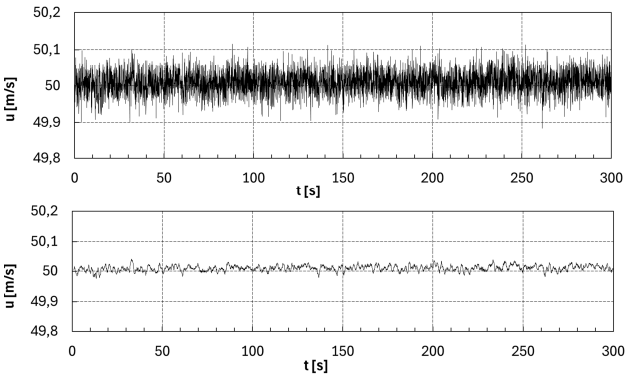

FIG 11. Speed variation over time at $50\mathrm{m/s}$. Upper pic: speed from raw pressure signals, lower pic: speed from $1\mathrm{s}$ floating average

7. ACKNOWLEDGEMENTS

I appreciate the financial support of UniBw M and the Faculty of Mechanical Engineering for funding this project. I would also like to thank Ralf Petz, Head of the BMW Aerodynamic Test Centre (AVZ) in Munich, Andreas Hauser, Head of RUAG Aerodynamics in Emmen, and Jürg Müller of RUAG Aerodynamics for the verification and provision of their wind tunnel design and operating data. It should be emphasised that the mechanical work was done by Eddie Kühlwein (UniBw M), hence special thanks to him for his patience and endurance.

DATA AVAILABILITY STATEMENT

The generated raw data are available on request from the corresponding author.

Contact address:

oliver.meyer@unibw.de
http://www.linkedin.com/company/unibw-mb

References

[1] William T. Eckert, Kenneth W. Mort, and Jean Jope. Aerodynamic design guidelines and computer program for estimation of subsonic wind tunnel performance. NASA Technical Note TN-D-8243, NASA, NASA Ames Research Center Moffet Field, CA, USA, Oct. 1974.

[2] R. D. Mehta and P. Bradshaw. Design rules for small low speed wind tunnels. *The Aeronautical Journal of the Royal Aeronautical Society*, pages 443–449, November 1979.

[3] P. Bradshaw and C. Pankhurst. The design of low speed wind tunnels. *Progress in Aerospace Sciences*, 5:1–69, 1964.

[4] Thomas Schuetz, editor. *Hucho - Aerodynamik des Automobils*. Springer Vieweg, Wiesbaden, 7 edition, 2023. ISBN: 978-3-658-35832-7. DOI: https://doi.org/10.1007/978-3-658-35833-4.

[5] B. F. R. Ewald, editor. *Wind Tunnel Wall Corrections, AGARD AG-336*. Canada Communications Group Inc.,

AGARD, BP-25,7 Rue Ancelle, F-92201 Neuilly-sur-Seine Cedex, France, October 1998. ISBN: 92-836-1076-8.

[6] O. Meyer and W. Nitsche. Progress in adaptive wind tunnel wall technology. *Progress in Aerospace Sciences*, 40:119–141, April 2004. DOI: https://doi.org/10.1016/j.paerosci.2004.02.001.

[7] Erich Truckenbrodt. *Fluidmechanik*, volume 2. Springer, Berlin, Heidelberg, 4th edition, October 2008. ISBN: 978-3-540-79023-5. DOI: https://doi.org/10.1007/978-3-540-79024-2.

[8] E. Wedemeyer and L. Lamarche. The use of 2d adaptive wall test sections for 3d flows. (AIAA 88-2041), 1988.

[9] I. E. Idelchik. *Handbook of Hydraulic Resistance*. Hemisphere Publishing Corporation, Washington, New York, London, 2 edition, 1986. ISBN: 3-540-15962-2.

[10] James H. Bell and Rabindra D. Mehta. Contraction design for small low-speed wind tunnels. Technical Report JIAA TR- 84, Stanford University, Department of Aeronautics and Astronautics, Stanford, CA 94305, April 1988.

[11] R. W. Fox and S. J. Kline. Flow regime data and design methods for curved subsonic diffusers. *JOURNAL OF BASIC ENGINEERING*, 84:303–312, April 1962.

[12] M. Kipek. Numerical analysis of three dimensional quadratic diffusers. Master thesis, Universität der Bundeswehr München, August 2016.

A. NASA WIND TUNNEL PERFORMANCE OUTPUT

PROGRAM "PERFORM"

* Windkanal Labor 5 PAGE 1

SINGLE-RETURN, CLOSED-TEST-SECTION WIND-TUNNEL PERFORMANCE

ATMOSPHERIC PRESSURE = .952 ATMOSPHERES = 96461.4 N/SQ. M
TEST SECTION CONDITIONS --
TOTAL PRESSURE = .952 ATMOSPHERES = 96461.4 N/SQ. M
TOTAL TEMPERATURE = 25.00 DEG C = 298.15 DEG K,
VELOCITY = 65.00 M/SEC = 126.35 KNOTS, DYNAMIC PRESSURE = 2341.32 N/SQ. M

NO.	SECTION TYPE	SHAPE	H1 H2 METERS	W1,D1 W2,D2 METERS	AREA1 AREA2 SQ M	A1/A0 A2/A0	AR,CR	2 THETA DEGREES	V1 V2 M/SEC	MACH1 MACH2	LENGTH METERS	DP/QL	DP/Q0
1	TEST SECT. DIFSN	RECT	.50	.50	.25	1.00	1.03	.26	65.0	.189	2.00	.04156	.04156
		RECT	.52	.50	.26	1.03			62.9	.182			
2	DIFFUSER	RECT	.52	.50	.26	1.03	2.48	9.39	62.9	.182	2.01	.07198	.06751
		RECT	.80	.80	.64	2.56			25.0	.072			
3	CONSTANT AREA DUCT	RECT	.80	.80	.64	2.56			25.0	.072	.50	.00703	.00106
		CIRC		.89	.63	2.51			25.5	.074			
4	FAN CONTRACTION	CIRC		.89	.63	2.51	1.46	41.84	25.5	.074	.20		
		CIRC		.89	.43	1.73			37.2	.108		.00179	.00059
5	FAN DUCT & STRUTS	CIRC		.89	.43	1.73			37.2	.108	1.15	.03639	.01208
		CIRC		.89	.43	1.73			37.2	.108			
6	CONSTANT AREA DUCT	CIRC		.89	.63	2.51			25.5	.074	.50	.00615	.00096
		RECT	.80	.80	.64	2.56			25.0	.072			
7	CORNER WITH VANES	RECT	.80	.80	.64	2.56			25.0	.072	.96	.17075	.02566
		RECT	.80	.80	.64	2.56			25.0	.072			
8	CONSTANT AREA DUCT	RECT	.80	.80	.64	2.56			25.0	.072	1.13	.01595	.00240

		RECT	.80	.80	.64	2.56			25.0	.072			
9	CORNER WITH VANES	RECT	.80	.80	.64	2.56			25.0	.072	.96	.17075	.02566
		RECT	.80	.80	.64	2.56			25.0	.072			

NO.	SECTION TYPE	SHAPE	H1 H2 METERS	W1,D1 W2,D2 METERS	AREA1 AREA2 SQ M	A1/A0 A2/A0	AR,CR	2 THETA DEGREES	V1 V2 M/SEC	MACH1 MACH2	LENGTH METERS	DP/QL	DP/Q0
10	DIFFUSER	RECT	.80	.80	.64	2.56	2.34	3.00	25.0	.072	9.15	.12853	.01932
		RECT	1.23	1.23	1.50	6.00			10.6	.031			
11	CORNER WITH VANES	RECT	1.23	1.23	1.50	6.00			10.6	.031	1.65	.17294	.00472
		RECT	1.23	1.23	1.50	6.00			10.6	.031			
12	CONSTANT AREA DUCT	RECT	1.23	1.23	1.50	6.00			10.6	.031	.40	.00395	.00011
		RECT	1.23	1.23	1.50	6.00			10.6	.031			
13	CORNER WITH VANES	RECT	1.23	1.23	1.50	6.00			10.6	.031	1.65	.17294	.00472
		RECT	1.23	1.23	1.50	6.00			10.6	.031			
14	CONSTANT AREA DUCT	RECT	1.23	1.23	1.50	6.00			10.6	.031	.50	.00494	.00013
		RECT	1.23	1.23	1.50	6.00			10.6	.031			
15	HONEYCOMB FLOW STR	RECT	1.23	1.23	1.50	6.00			10.6	.031	.05	.18155	.00495
		RECT	1.23	1.23	1.50	6.00			10.6	.031			
16	SCREEN, WIRE MESH	RECT	1.23	1.23	1.50	6.00			10.6	.031		1.97036	.05375
		RECT	1.23	1.23	1.50	6.00			10.6	.031			
17	SCREEN, WIRE MESH	RECT	1.23	1.23	1.50	6.00			10.6	.031		1.97036	.05375
		RECT	1.23	1.23	1.50	6.00			10.6	.031			
18	SCREEN, WIRE MESH	RECT	1.23	1.23	1.50	6.00			10.6	.031		1.97036	.05375
		RECT	1.23	1.23	1.50	6.00			10.6	.031			

19 CONSTANT AREA DUCT	RECT	1.23	1.23	1.50	6.00			10.6	.031	.60	.00592	.00016
	RECT	1.23	1.23	1.50	6.00			10.6	.031			
20 CONTRACTN. SINGLE	RECT	1.23	1.23	1.50	6.00	6.00	36.59	10.6	.031	1.24		
	RECT	.50	.50	.25	1.00			65.0	.189		.00823	.00823

TOTAL CENTERLINE LENGTH = 24.64 METERS

PERFORMANCE SUMMARY --
TOTAL PRESSURE LOSS (DP/Q0) = .38108 ENERGY RATIO = 2.624
TOTAL POWER --

INPUT TO FLOW	OUTPUT REQUIRED	AVERAGE PER FAN	FAN EFFICIENCY	TOTAL NUMBER OF FANS
14327. WATTS	18851. WATTS	18851. WATTS	76.00 PERCENT	1.

MAXIMUM VELOCITY FOR A SPECIFIED POWER CONSUMPTION

THE MAXIMUM TEST SECTION FLOW ACHIEVABLE WITH 22000. WATTS OF POWER AVAILABLE IS APPROXIMATELY AS FOLLOWS --
VELOCITY -- 68.51 M/SEC = 133.17 KNOTS
MACH NUMBER -- .20
DYNAMIC PRESSURE -- 2595.85 N/SQ M

WIND-TUNNEL CIRCUIT CHARACTERISTICS SUMMARY
TAKEN AT DOWNSTREAM END OF EACH SECTION

SECTION ASSIGNED SEQUENCE	CUMULATIVE CIRCUIT LENGTH METERS	MACH NUMBER	CUMULATIVE PRESSURE LOSS (DP/Q0)	Cp
1	2.00	.182	.04156	-.986
2	4.01	.072	.10907	-.259
3	4.51	.074	.11013	-.266
4	4.71	.108	.11072	-.443
5	5.85	.108	-.25828	-.077
6	6.35	.072	-.25732	.106
7	7.31	.072	-.23165	.080
8	8.44	.072	-.22926	.078
9	9.40	.072	-.20359	.052
10	18.55	.031	-.18427	.157
11	20.20	.031	-.17956	.152
12	20.60	.031	-.17945	.152
13	22.26	.031	-.17473	.147
14	22.76	.031	-.17460	.147
15	22.81	.031	-.16964	.142
16	22.81	.031	-.11589	.089
17	22.81	.031	-.06214	.035
18	22.81	.031	-.00839	-.019
19	23.41	.031	-.00823	-.019
20	24.64	.189	0.00000	-1.009